Video Article

Scanning Skeletal Remains for Bone Mineral Density in Forensic Contexts

Amanda R. Hale[1], Ann H. Ross[1]

[1]Department of Biological Sciences, North Carolina State University

Correspondence to: Amanda R. Hale at arhale@ncsu.edu

URL: https://www.jove.com/video/56713
DOI: doi:10.3791/56713

Keywords: Medicine, Issue 131, Bone mineral density, BMD, skeletal remains, fatal starvation, child neglect, dual-energy x-ray absorptiometry, DXA, survivability, forensic anthropology

Date Published: 1/29/2018

Citation: Hale, A.R., Ross, A.H. Scanning Skeletal Remains for Bone Mineral Density in Forensic Contexts. *J. Vis. Exp.* (131), e56713, doi:10.3791/56713 (2018).

Abstract

The purpose of this paper is to introduce a promising, novel method to aid in the assessment of bone quality in forensically relevant skeletal remains. BMD is an important component of bone's nutritional status and in skeletal remains of both juveniles and adults, and it can provide information about bone quality. For adults remains, it can provide information on pathological conditions or when bone insufficiency may have occurred. In juveniles, it provides a useful metric to elucidate cases of fatal starvation or neglect, which are generally difficult to identify. This paper provides a protocol for the anatomical orientation and analysis of skeletal remains for scanning via dual-energy X-ray absorptiometry (DXA). Three case studies are presented to illustrate when DXA scans can be informative to the forensic practitioner. The first case study presents an individual with observed longitudinal fractures in the weight bearing bones and DXA is used to assess bone insufficiency. BMD is found to be normal suggesting another etiology for the fracture pattern present. The second case study employed DXA to investigate suspected chronic malnutrition. The BMD results are consistent with results from long bone lengths and suggest the juvenile had suffered from chronic malnutrition. The final case study provides an example where fatal starvation in a fourteen-month infant is suspected, which supports autopsy findings of fatal starvation. DXA scans showed low bone mineral density for chronological age and is substantiated by traditional assessments of infant health. However, when dealing with skeletal remains taphonomic alterations should be considered before applying this method.

Video Link

The video component of this article can be found at https://www.jove.com/video/56713/

Introduction

The objective of forensic anthropological analyses relies on the practitioner's understanding of bone as a complex tissue with multiple units and variation. Bone is a hierarchical, composite tissue with both organic and inorganic components organized into a matrix of collagen and carbonated apatite[1,2,3,4]. The inorganic component, or bone mineral is organized in a nanocrystalline structure to provide stiffness and framework for the organic portion[1,2,5]. The mineral aspect comprises approximately 65% of bone by weight and its' mass is influenced by both genetic and environmental factors[1,2,4,6]. Because bone mineral occupies a three-dimensional space, it can be measured as bone mineral density (BMD), or a function of the mass and the volume occupied[7]. The bulk density of bone mineral varies with age from birth into adulthood[8,9,10,11,12] and has been used extensively in clinical settings as an indicator of osteoporosis and fracture risk[4,13,14,15,16,17,18]. Dual-energy X-ray absorptiometry (DXA) has been a widespread tool for the assessment of bone health since its introduction in 1987, particularly scans performed in the lumbar spine and hip regions[11,13,19]. Validation of DXA scans has been shown as the gold standard when investigating changes in BMD[13,19,20,21,22,23]. Subsequently, the World Health Organization (WHO) has created normative standards including *t*- and *z*-score definitions for juvenile and adult lumbar spine (L1-L4) and hips as these are the regions easily captured volumetrically[11,13,19,24].

The increasing reliance on forensic anthropology in medicolegal casework has encouraged the investigation of novel techniques to better assess skeletal remains in a variety of circumstances. Among these potential techniques is the application of DXA scans to assess BMD as an indicator of bone quality in cases involving fatal starvation and neglect in juveniles[25,26], identification of metabolic bone diseases, and estimating survivability of skeletal elements in taphonomic research[7,27].

In the 2015 U.S. Department of Health and Human Services Child Maltreatment Report, 75.3% of the reported child abuse cases were some form of neglect with ~1,670 fatalities resulting from fatal starvation and neglect in 49 states[28]. Most juvenile victims of neglect fail to show signs of external physical abuse, but *failure-to-thrive* is seen in all cases[29,30]. *Failure-to-thrive* is defined as the inadequate nutrition intake to support growth and development. These can have different factors, one of which is neglect resulting from nutritional deprivation[25,31] (see Ross and Abel[32] for a more comprehensive review). Deliberate starvation that results in the death of a child or infant is much rarer and considered as the most extreme form of maltreatment[25,33,34]. These nutritional deficiencies have a significant effect on bone growth, particularly longitudinal growth in children as an immediate consequence of malnutrition[35]. Skeletal growth and mineralization primarily depend on vitamin D and calcium, and their supplementation has been linked to increased BMD[25,35,36].

It is exceedingly difficult to identify or prosecute these cases even following a complete autopsy[31,37,38] and special consideration to methods employed must be used. Thus, in cases where fatal starvation or malnutrition is suspected, a multidisciplinary approach is needed particularly

in cases involving remains in advanced states of decomposition[26]. When skeletal remains are involved, bone densitometry is a useful tool in conjunction with other skeletal indicators such as dental development, measurement of the *pars basilaris* of the skull, and long bone lengths[26]. Without using the skeletal indicators mentioned above for infants and juveniles, it would not be possible to discern if low BMD is the result of an inherent metabolic disorder, malnutrition, or taphonomic process. Another concern is the estimation of body size (weight and stature) in infant or juvenile skeletal remains. Most normative data sets require information about height or weight for comparison purposes as bone growth in children is size and age dependent[12]. When the remains being assessed are unidentified, estimation methods should be employed. For infants under one, normative DXA data is age matched only. In juveniles over the age of 1, Ruff[39] or Cowgill[40] are recommended for estimating body size in skeletal remains as they are based on the Denver Growth Study sample including ages 1 - 17[39,40]. When age and body size are estimated, confidence intervals vary and comparison of the mean to the Center for Disease Control (CDC) produced growth curves[41] should be included in the report as well as the confidence interval for the estimated body size. It is important to note that in most cases, information regarding ancestry and sex cannot be determined from juvenile skeletal remains prior to puberty, which is particularly important for adolescents as ancestry and sex are known to significantly impact BMD in adults. In these circumstances, the DXA method may not be applicable. In identified cases, biological information regarding ancestry, sex, and body size, should be obtained prior to analysis.

Bone densitometry in pediatrics has increased with the development of normative data[42,43] with DXA being the most widely available technique[44]. Malnourished children show significantly lower levels in BMD than healthy children with mineralization correlated with severity of malnutrition[45]. DXA scans of the lumbar spine and hips are the most appropriate areas to assess for juveniles according to The American College of Radiology[46]. Reproducibility has been shown for spine, whole hip, and whole body in children throughout the growth period[47]. However, the lumbar spine is preferred as it is primarily composed of trabecular bone, which is more sensitive to metabolic changes during growth and has been found to be more precise than whole hip assessments[25,47,48]. Using DXA scans is common in pediatric assessment. However, since DXA is two-dimensional, it does not capture true volume and produces a BMD based on bone area[13]. In children, this is an important distinction as body and bone size vary within and between age groups in children[12]. Most normative data available is for comparison with DXA measurements, but care should be exercised to choose an appropriate reference population (see Binkovitz and Henwood[13] for a list of commonly used DXA normative databases).

Following the scan, a *z*-score is calculated using an age-matched and population specific reference sample. *Z*-scores are more appropriate for juveniles since *t*-scores compare the measured BMD to a young adult sample[12]. A *z*-score between -2 to 2 indicates normal BMD for chronological age while any score below -2 indicates low BMD for chronological age[49]. The -2 to 2 range for both the *t*- and *z*-score represent up to two standard deviations from the mean. Plainly, if a measured BMD score is within two standard deviations above or below their reference population mean, they are considered clinically normal.

The reliance on morphological variation for the forensic anthropologist comes from many sources. One of which is the skeletal variation that arises from disease processes, including metabolic bone disorders[50]. The ability to identify specific disorders in skeletal remains has a two-fold advantage: 1) adding information to the biological profile making it more robust and 2) identifying if fractures are pathological or the result of inflicted trauma. There are a variety of metabolic bone disorders[51,52,53], but the most relevant for BMD measures of contemporary remains is osteoporosis. Osteoporosis develops when the rate of trabecular bone loss is greater than the rate of cortical bone loss with a net loss in bone density[53,54,55]. Trabecular bone loss is correlated to an increased risk of fracture, especially in bones that have greater trabecular bone content (*e.g.*, the os coxa)[4,55].

Numerous studies on osteoporosis and bone mineral density in skeletal remains have been conducted on archaeological assemblages using both DXA[56,57,58,59] and other methods[60,61,62]. However, when assessing osteoporosis in the adult skeleton from archaeological contexts, practitioners disregard that diagnosing osteoporosis clinically requires the mean of a younger reference sample contemporaneous with the individuals being assessed[55,63,64]. This is not an issue in forensic anthropology contexts since individuals are age- and sex- matched to modern populations with developed reference samples for both the hip and the lumbar spine, although changes in BMD through diagenesis should be considered for forensic remains. However, taphonomy is the likely factor affecting the ability to obtain legitimate BMD measures from archaeological samples. This is a consideration in forensic contexts as well, where remains recovered from burial conditions with potential postmortem intervals beyond a few months. While still of forensic interest, sufficient doubt could be raised for any BMD scores obtained from remains found in these circumstances.

Osteoporosis is clinically assessed using *t*-scores of BMD measures that are derived from the individuals' BMD measures in the hip or lumbar spine relative to a young adult reference sample using DXA[65,66,67,68]. This reference sample can be employed for identifying the occurrence of osteoporosis in the skeleton. In forensic contexts, this is useful for two reasons: 1) differentiating between fractures related to abuse-inflicted trauma in the elderly and those from increased bone fragility in osteoporotic individuals[69], and 2) as a possible personal identification feature[50].

Bone density has long been considered an indicator that reflects the activity and nutrition of an animal[70,71]. More recently it has been noted that bone density, as an intrinsic property of bone, affects its survivability during taphonomic processes[7]. A consequence of decomposition is the differential survivability of skeletal elements (*i.e.*, discrete, anatomically complete units of the skeleton) and bone density can be used as a predictor of survivability, or bone strength[7,70,71,72,73,74,75]. This is important in forensic contexts as well as archaeological and paleontological environments in that it affects the practitioners' ability to adequately employ methods to estimate a biological profile (or age, sex, stature, and ancestry) if only certain skeletal elements are represented.

Bulk density (bone density with pore space included in the measurement) is the appropriate measurement in this situation, considering it is precisely the porous structure of bone that influences its susceptibility to taphonomic processes[7]. Many methods of assessing bone density have been employed including single-beam photon densitometry[27,75], computed tomography[76,77,78], photodensitometry[72,79], and DXA[80,81,82]. DXA scans may be preferable to other methods as it is relatively inexpensive, whole body scans can be performed, and individual skeletal elements can be assessed separately or together during analysis. Using BMD scans before and after taphonomic research studies provides useful information on bone survivability resulting from different taphonomic factors and environments[82].

This paper outlines a protocol for obtaining DXA scans of skeletal remains. The method employs the common, clinical positioning of individuals when performing lumbar spine and hip scans. This allows practitioners to compare the skeletal remains with the appropriate normative standards. The protocol outlined is applicable to both juvenile and adult remains with limitations discussed later.

Protocol

The protocol herein adheres to the North Carolina State University's ethics guidelines for human research.

1. Machine Preparing

NOTE: The following protocol can be broadly applied to any whole body, clinical DXA and BMD scanner.

1. Perform calibration once daily prior to scanning any individuals to ensure quality control. After calibration prompts appear upon start-up of the systems' software, scan a lumbar spine phantom of known density to ensure correct reading of the BMD scanner.
2. If the scanner being utilized does not have a quality control feature in the software, compare the lumbar spine results with those recorded on the spine phantom to ensure the correct measurements.
   NOTE: The spine phantom, should be placed in the center of the scan table and lumbar spine should be selected for quality control.
3. Perform additional tests (*e.g.*, radiographic uniformity) as needed. Perform radiographic uniformity every ten scans maximum to ensure that the entire scanning surface is detected by the scanner.
4. If the scanner being utilized does not have a radiographic uniformity test in the quality control menu, select whole body scan to ensure the scanner can read the entire scanning surface.
   NOTE: Always center the exam table following quality control and before performing exams.

2. Performing Exam

1. Create patient profiles
   1. Create new patient profiles for each new individual scanned to maintain chain of custody and to ensure scans are correctly associated with individual remains. If the individual being scanned is identified, proceed to step 2.1.2. If the individual is unidentified, establish the biological profile prior to scanning to employ the most accurate database references.
   2. Enter demographic information into the patient profile including estimated stature if unknown. Ensure that you select the most appropriate equation for the remains being investigated.
   3. Select scan type. For steps 2.2, select Anterior-Posterior (AP) Lumbar Spine. For step 2.3, select Left or Right Hip scans.

2. AP Lumbar Spine scan
   NOTE: Require lumbar vertebrae (L) one to four.
   1. Select **Perform Exam | choose patient | Select scan type |AP Lumbar Spine | Next**. Select an open container at least as large as the articulated segment of L1-L4.
      NOTE: The one used in this study is 48.26L X 26.85W X 8.89D in cm (19 in. L X 10.57 in. W X 3.5 in. D).
   2. Fill the bottom of the container with rice as a soft tissue proxy.
      NOTE: Any kind of rice can work as a soft tissue proxy.
   3. Place L1-L4 in anatomical position (spinous processes should be oriented downwards) in the rice with approximately 0.7 cm (0.28 in.) between each vertebral body as shown in **Figure 1A**. Ensure that the superior and inferior articular facts are articulated, but the vertebral bodies are not in contact with one another.
   4. Center the scanning table and place the container with L1 is oriented towards top (head) of scanning table and L4 is placed 1 cm superior to the intersecting crosshairs. The vertical laser line should be bisecting the vertebrate bodies of all four vertebrae (**Figure 1B**).
   5. Cover the exposed bone with rice.
   6. Select **Start Scan**.
   7. Proceed to analysis (step 3.1), If scanned properly (**Figure 2**). Repeat the scan if not all vertebrae are captured.

3. Left or Right Hip scans
   NOTE: **Figure 3** is from a left hip exam, if performing a right hip exam, positioning is mirrored.
   1. Select **Perform Exam | choose patient | Select scan type | Left Hip (or Right Hip) | Next**. Select an open container at least as large as the articulated os coxa and femur being scanned.
      NOTE: The one used in this study is 88.5L X 41.5W X 13.9D in cm (34.85 in. L X 16.35 in. W X 5.47 in. D).
   2. Fill the bottom of the container with rice (any kind of rice will work as a soft tissue proxy).
   3. Place the os coxa with the acetabulum and obturator foramen facing laterally with the pubic bone oriented medially. Position the ischial tuberosity beneath the femoral head as it articulates with the acetabulum (**Figure 3A**).
      NOTE: Positioning of the ischial tuberosity is most important because if it extends laterally below the femoral neck it will inflate BMD estimates.
   4. Place the femur with the femoral head in the acetabulum and with the greater trochanter and femoral head in line parallel to the scanning table (*i.e.*, in the same plane). Ensure that the femoral shaft is medially rotated with the distal condyle rotated medially and slightly higher than the medial condyle (**Figure 3B**).
   5. Center the scanning table, then move the position of the scanning arm and table until the laser crosshairs are oriented so that the center is directly above the subtrochanteric area of the femur with the vertical line bisecting the top-half of the femoral shaft (**Figure 3A**). Do not move the remains once they have been positioned. Move the table ensures that bones remain in proper anatomical position.
   6. Cover the remaining visible portion of the femoral-acetabular joint with rice.

7. Select **Start Scan**.
8. Proceed to analysis in step 3.2 if scanned properly (**Figure 4**).
   NOTE: Scans should capture the alignment of the joint such that the midline of the proximal femur is in one plane. The midline should lie from the center of the femoral head to just under the greater trochanter.

3. Analyzing Exams

1. Analyze AP Lumbar Spine scan
   1. Following the scan, an Exit Exam prompt box will appear. Select **Analyze Scan**.
      NOTE: Software will separate each vertebra into their own regions to assess individual elements and total BMD when scanned properly as shown in **Figure 5**.
   2. Select **Results** in the **Scan Analysis** window. Select vertebral lines If the vertebrae are not properly separated for minor adjustments or directly reposition vertebrae for rescanning.
   3. Obtain both age-matched and population specific BMD reference measures to calculate a *z*-score when performing juvenile BMD scans.
   4. Collect results graph for visualization of the individual relative to the reference population.
      NOTE: **Figure 6** shows scan results for AP Lumbar Spine of a 31-year-old female.

2. Analyze hip scan.
   1. Following the scan, an Exit Exam prompt box will appear. Select **Analyze Scan**.
      NOTE: Software will automatically capture the femoral neck, Ward's triangle, and trochanteric area as shown in **Figure 7**, if scanned properly.
   2. Select the bone map tool to add or delete areas that are not part of the femoral neck and trochanteric region when not read exactly by the software due to slight malposition. Make midline adjustments directly on scan by selecting the neck tool and repositioning the midline.
   3. Reposition and rescan if these small adjustments do not allow the proper alignment shown in **Figure 7**.
   4. Select **Results** in the **Scan Analysis** window. Compare to reference data for femoral neck, trochanteric region, and the intertrochanteric region in the software for adults.
   5. Compare results with the appropriate age- and population-matched references when assessing juveniles.
   6. Use the *t*-score for adults as it is the most appropriate to differentially assess pathological conditions.
      NOTE: **Figure 8** shows the ideal scan results for the left hip analysis of a 31-year-old female.

Representative Results

The methodology proposed here is commonly used in living patients and consideration of its novelty to deceased individuals should be noted. **Figure 6** and **Figure 8** present the results of an AP lumbar spine and left hip scan, respectively. The individual assessed in these scans is a deceased white, female, 31 years of age that is housed at the Forensic Analysis Laboratory of North Carolina State University. This individual had a total BMD score of 0.944 g/cm^2 with a corresponding *t*-score (*-0.9*) for the ancestry and sex-matched reference population. According to the WHO classification, her BMD score is clinically normal and not below the -2 *t*-score that suggests a BMD consistent with osteoporosis/ increased fracture risk[8,83]. The results presented are from three forensic cases where BMD scores were used to assess different etiologies in each individual set of remains. The methodology proposed has not been systematically assessed in skeletal remains, but in combination with other methods can aid the investigator during their assessment. *Case study 1* illustrates its use in adults whereby perimortem, longitudinal cracking is evident in the long bones. BMD scores were used to assess whether this cracking was due to fracture risk during life or postmortem processes where color change comparison was not applicable. *Case study 2* illustrates its use in juvenile remains when long-term abuse and neglect are suspected. *Case study 3* illustrates the method's use in infant deaths when fatal starvation is suspected.

In *Case Study 1*, this individual was a 40-year-old male exhibiting a rare fracture series that includes longitudinal fractures of both anterior surfaces of the femur and tibia that completely penetrated the cortical bone in the center of each bone (**Figure 9A** and **9B**). The longitudinal fractures are also associated with transverse fractures bisecting the anterior portion of the tibia at midshaft and slightly distal. As there are no signs of healing, but no differences in coloration, traditional fracture timing methodologies to distinguish peri- and postmortem were inconclusive. Moreover, there are pathological changes that have been observed in living diabetes patients including a visible loss of trabecular bone that can be observed in the individual's radiographs (**Figure 9A**). To assess if the acute fractures present in the lower limb bones were the result of fracture fragility or more simply, a postmortem artifact from natural drying processes[80], a DXA scan of the left hip was obtained (**Figure 10**). The left hip is assessed since the longitudinal fractures were observed in the femora and tibiae and the lumbar spine was incomplete. The approach here was to ascertain if the BMD was sufficiently low that normal weight-bearing activities could cause the fractures observed. Total BMD was 1.299 g/cm^2 with a corresponding *t*-score of *1.8* indicating bone insufficiency was not the cause of the longitudinal fractures. In addition, postmortem longitudinal cracking produces fracture lines that run along the grain of the bone and can produce fractures at perpendicular angles from one another[84].

In *Case Study 2*, **Figure 11** provides the results for a 13-year-old, female recovered from a clandestine grave with a suspected history of long-term abuse. Numerous antemortem fractures were evident and patterning was consistent with child abuse[85]. Current standards to assess malnutrition in juveniles include comparison of long bone lengths to a reference sample. The juvenile limb lengths for this individual were *355 mm* and *300 mm* for the left femur and tibia, respectively. These lengths are size-matched most closely with 9-year-old mean lengths (*350 mm* and *280 mm* for femora and tibiae, respectively). This is consistent with a pronounced growth deficit for this individual[86,87]. Ruff's[39] equation for femur and tibia lengths was used to estimate juvenile stature for the decedent. The estimated stature was 53.3 inches (136.2 cm) (95% CI: 51.1-55.5 inches). This was compared to the CDC 2000 growth curves for girls aged 2-20[41]. As seen in **Figure 12**, the decedent lies below the 3rd percentile for stature-for-age suggesting delayed growth well below most U.S. 13-year-old females. BMD was assessed to provide further

insight into the degree of malnutrition as the association between BMD loss and poor nutrition is well established[25,35,36]. The lumbar spine was chosen for its completeness and larger composition of trabecular bone. The total BMD of the AP lumbar spine was measured at *0.660 g/cm*^{2} with a *z*-score of *-2.2* from the manufacturer's database. The manufacturer's database is an age and sex matched sample containing 1,948 individuals aged 3-20 years[88]. This *z*-score is consistent with *low BMD for chronological age* providing further evidence consistent with chronic malnutrition (**Figure 13**).

In *Case Study 3*, **Figure 14** displays the BMD results of the lumbar spine for a 14-month-old infant with starvation suspected as the cause of death. The remains were still in early fresh stage of decomposition so articulation of epiphyses was not a concern and weight was 6.1 kg (13.4 lbs). For comparison purposes, the Gomez and colleagues and Waterlow classification systems were employed to estimate malnutrition from reference height and age measurements. Following the Gomez and colleagues[89] equation:

Percent of reference weight for age = ((patient weight) / (weight of normal child of same age)) * 100

where the weight of normal child of same age is taken from a reference population. The infant in this case measured at 38% weight for age of the reference sample from Gomez and colleagues[89], which is equivalent to Grade III (severe malnutrition). The Waterlow[90] classification system places 38% as severe wasting, but without stunting as height was within the normal range. The total BMD was measured at *0.190 g/cm*^{2} while the age-matched reference group has an average total BMD of the lumbar spine of *0.399 +/- 0.040 g/cm*^{2} [45]. The *z*-score was calculated as:

z-score = ((Measured BMD - Age Matched Mean BMD) / Population SD)

and was *-5.225* with the age-matched mean from a 1-year-old reference population of 40 infants. The reference data was produced from a longitudinal study by Braillon and coworkers[91] that has been validated in the literature for DXA spine BMD measures[49,92]. Moreover, a study by Gallo and colleagues suggests the infant BMD observed is below the 3rd percentile of spine BMD for age for 12-month olds[92]. Any score below -2 is considered low BMD for chronological age placing the infant in the 0.1 percentile of the normal population (**Figure 13**). For comparison, the weight of the infant (6.1 kg) was plotted on the CDC 2000 growth curve chart for males aged 0-3[41]. As seen in **Figure 15**, the infant falls well below the 3rd percentile for weight-for-age, which is consistent with the DXA *z*-score well below the *-2* for the low end of normal individuals.

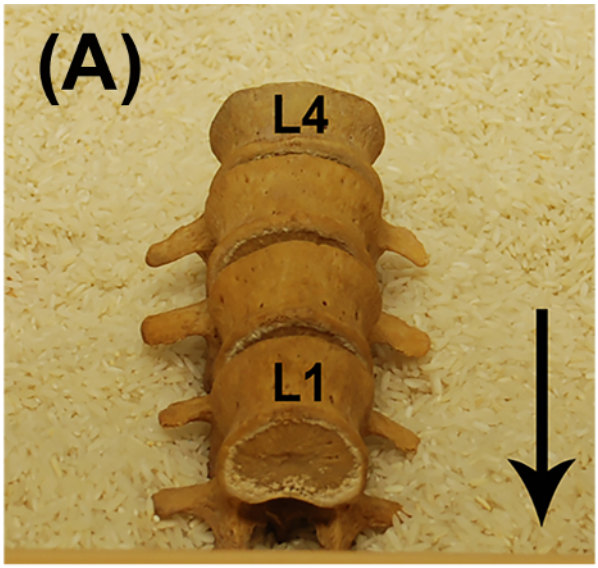

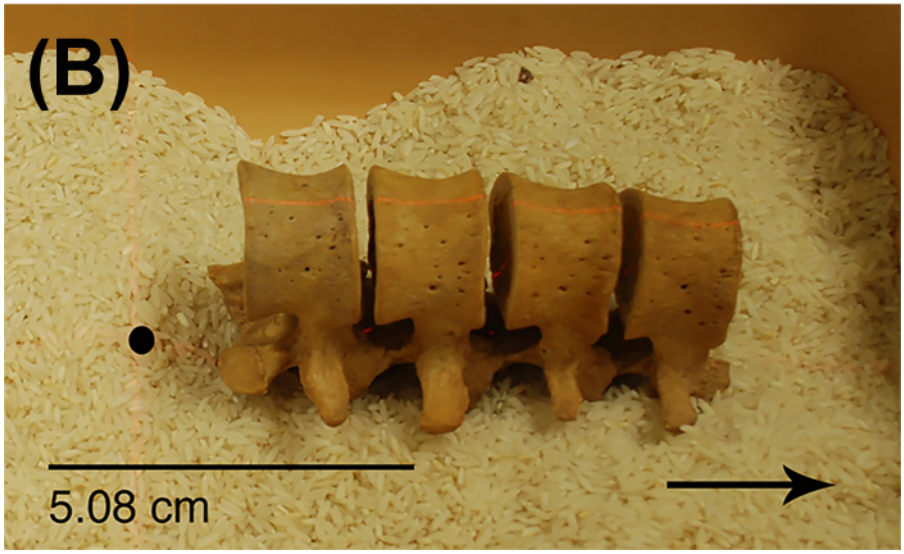

Figure 1: Orientation and placement of lumbar spine segments, L1-L4 for scanning: (A) shows proper orientation for scanning with spinous processes oriented downwards (corresponds to step 2.2.3); (B) correct location for scanning with laser line bisecting vertebrate bodies and no contact between vertebrate bodies and black dot represents the crosshairs (corresponds to step 2.2.4). Arrow indicates direction to head of scanner. Please click here to view a larger version of this figure.

Figure 2: Successful AP lumbar spine scan ideal for analysis. Corresponds to step 2.2.7.

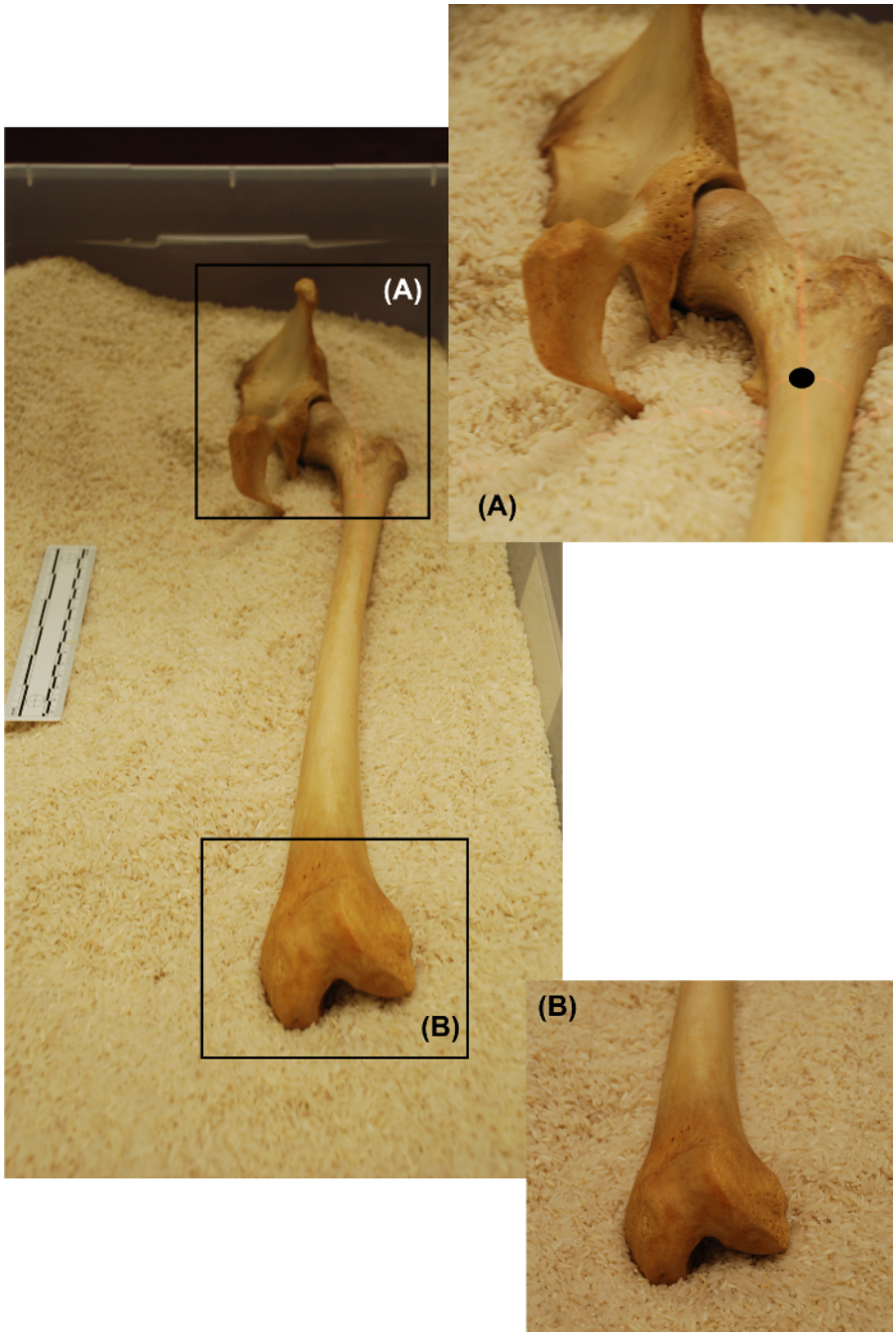

Figure 3: Placement of hip joint (os coxa and femur) to recreate acetabulo-femur joint. (A) indicates the hip joint alignment for scanning with the femoral head in the acetabulum and femoral head and greater trochanter in the same plane parallel to the scanning table (step 2.3.3) and the black dot indicates the location of crosshairs for correct table placement (step 2.3.5). (B) illustrates the degree of medial rotation of the femur appropriate for scanning (step 2.3.4). Please click here to view a larger version of this figure.

Figure 4: Successful left hip scan ideal for analysis. Notice that the os coxa does not extend below the femoral neck. Ensure placement of the joint does not have the iliac tuberosity inferior to the femoral neck (step 2.3.8).

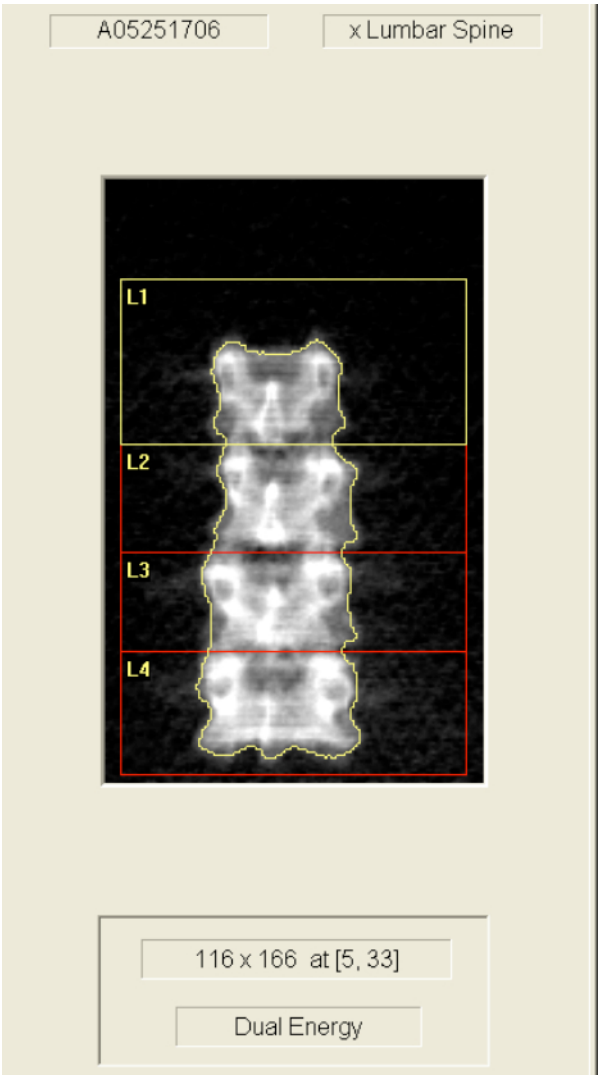

Figure 5: An example of a successful AP lumbar spine scan. L1 - L4 indicates proper placement of vertebral lines between each vertebra (step 3.1.1).

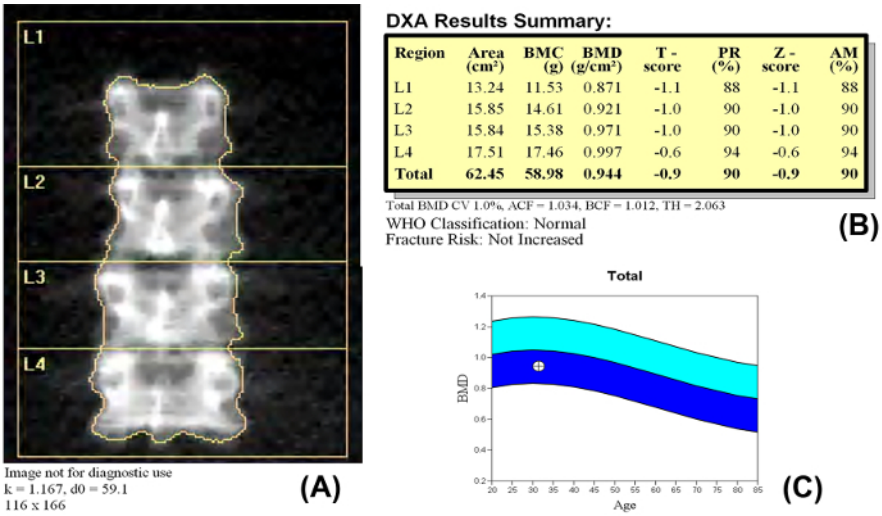

Figure 6: BMD results from an AP lumbar spine analysis (step 3.1.4). The results presented here are from a deceased white female, 31 years of age, and 64 inches tall. Report has been anonymized for publication. (A) presents image of properly scanned lumbar vertebrae separated by software placed vertebral lines; (B) scan results listing the individual vertebrae and total BMD scores as well as the *t*- and *z*-scores for the individual. The *t*- and *z*-scores were obtained using the WHO reference database for white females; (C) BMD vs. Age graph represents where the individual's BMD score (cross-hatch circle) falls within the range of average adult females in the WHO database.[83] The darker blue shading represents the acceptable range above the mean and the lighter blue shading represents the acceptable range below the mean, or the two tails of the bell curve around the mean in a normal distribution curve. Please click here to view a larger version of this figure.

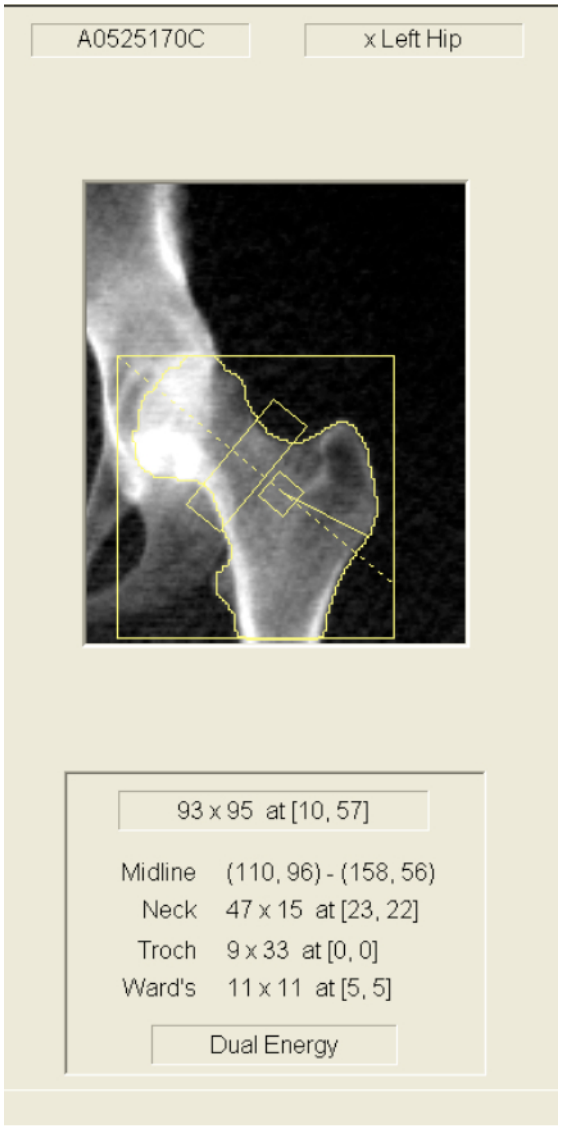

Figure 7: Screen displays an example of a successful hip scan with the femoral midline bisecting the femoral head to just inferior the trochanteric region. The femoral neck box should be at an angle to capture the full femoral neck angle (step 3.2.2).

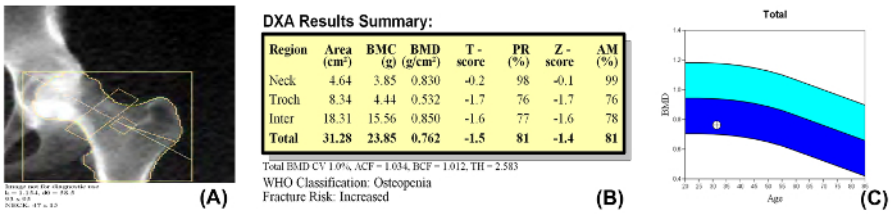

Figure 8: BMD results from a left hip analysis (step 3.2.5). The results presented here are from a deceased white female, 31 years of age, 64 inches tall. Report has been anonymized for publication. (A) presents image of properly scanned left hip with midline accurately placed with no additional bone included from os coxa; (B) scan results listing the neck, trochanteric region (Troch), the intertrochanteric region (Inter), and total BMD scores as well as the *t*- and *z*-scores for the individual. The *t*- and *z*-scores were obtained using the WHO reference database for white females. This individual is classified as osteopenic with increased fracture risk using the WHO references[83]; (C) BMD vs. Age graph represents where the individual's BMD score (cross-hatch circle) falls within the acceptable range albeit on the low end of peak adult females in the WHO database. The darker blue shading represents the acceptable range above the mean and the lighter blue shading represents the acceptable range below the mean, or the two tails of the bell curve around the mean in a normal distribution curve. Please click here to view a larger version of this figure.

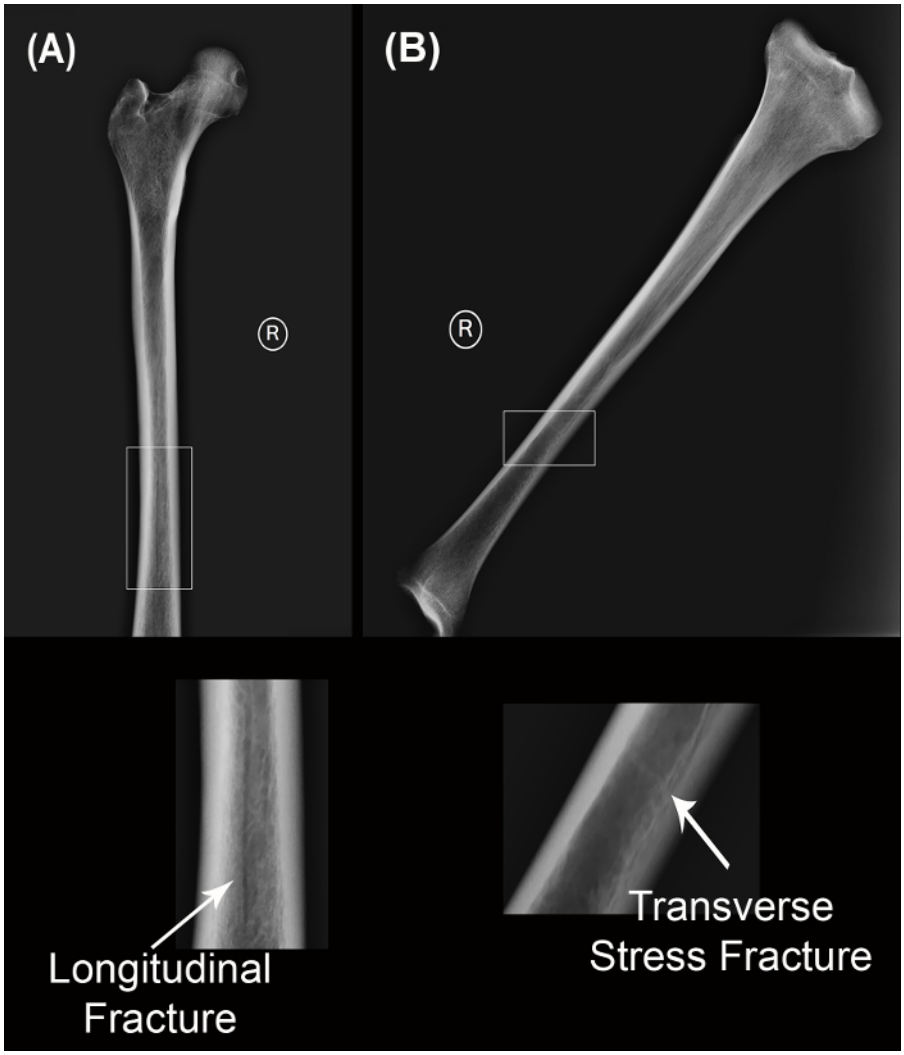

Figure 9: Radiographs for *Case Study 1*. (A) shows the longitudinal fractures of the right femur and (B) the transverse stress fracture of the right tibia. Also note the reduced radiopaque quality of the proximal femur. Please click here to view a larger version of this figure.

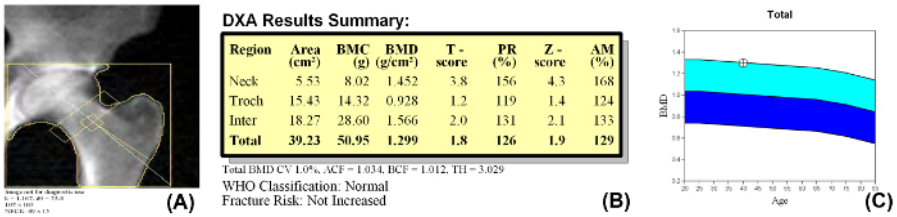

Figure 10: BMD results for *Case Study 1*. The results presented here are from a deceased white male, 40 years of age, approximately 72 inches tall. Report has been anonymized for publication. (A) presents image of left hip scan; (B) scan results presenting the neck, trochanteric region (Troch), the intertrochanteric region (Inter), and total BMD scores as well as the *t*- and *z*-scores for the *Case Study 1*. The *t*- and *z*-scores were obtained using the WHO reference database for white males.[83] This individual is classified as normal using the WHO references; (C) BMD vs. Age graph represents where the individual's BMD score (cross-hatch circle) falls within the acceptable range of adult males in the WHO database. The darker blue shading represents the acceptable range above the mean and the lighter blue shading represents the acceptable range below the mean, or the two tails of the bell curve around the mean in a normal distribution curve. Please click here to view a larger version of this figure.

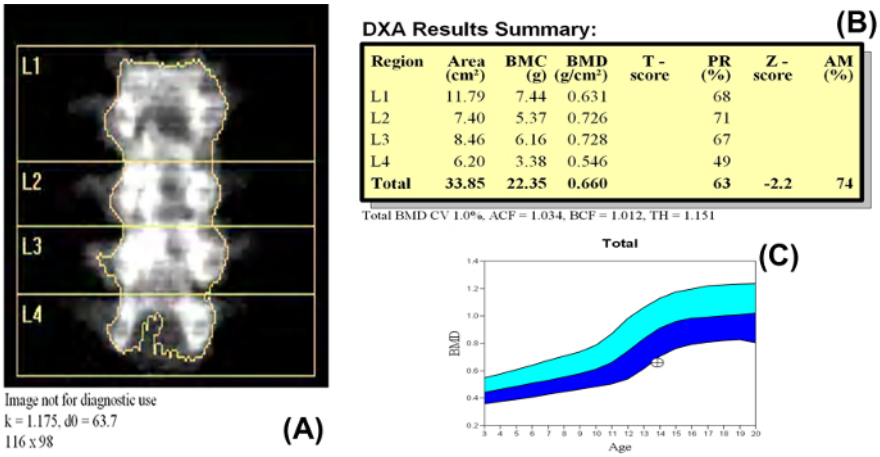

Figure 11: BMD results for *Case Study 2*. The results presented here are from a deceased white female, 13 years of age, approximately 53 inches tall. Report has been anonymized for publication. (A) presents scan of AP lumbar vertebrae for *Case Study* 2 separated by software placed vertebral lines; (B) scan results present the individual vertebrae and total BMD scores as well as the *z*-scores for the individual. *Z*-scores only are presented in juvenile cases because they were obtained using the WHO reference database for age- and sex-matched individuals; (C) BMD vs. Age graph represents where the individual's BMD score (cross-hatch circle) falls below the range (*z*-score=-2.2) of 13-year-old white females in the manufacturer's database.[88] The darker blue shading represents the acceptable range above the mean and the lighter blue shading represents the acceptable range below the mean, or the two tails of the bell curve around the mean in a normal distribution curve. Please click here to view a larger version of this figure.

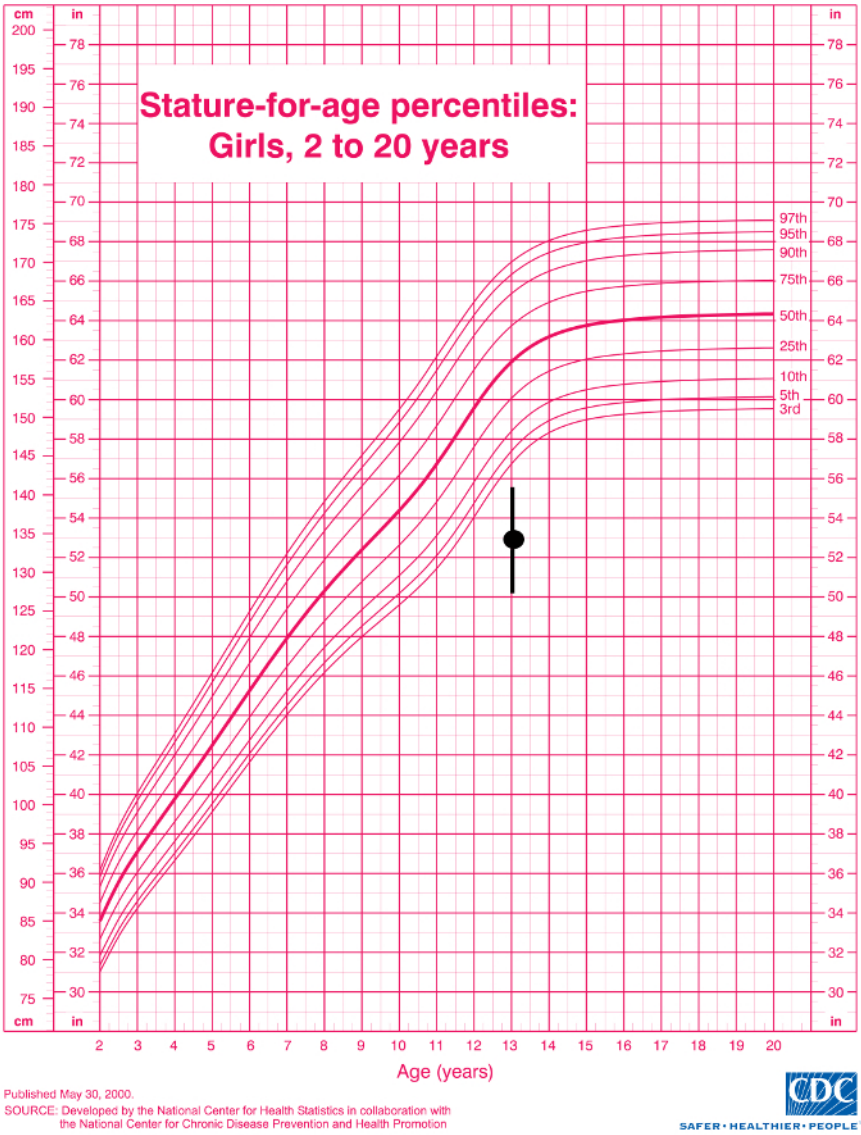

Figure 12. Individual growth chart 3rd, 5th, 10th, 25th, 50th, 75th, 90th, 95th, 97th percentiles, 2 to 20 years: Girls stature-for-age

Figure 12: Growth chart illustrating the delayed maturation of the 13-year-old female decedent.[41] The black dot represents the mean estimated stature and the black lines represent the 95% confidence interval for the stature equation. The individual lies below the 3rd percentile for stature-for-age within the entire range of the CI. Please click here to view a larger version of this figure.

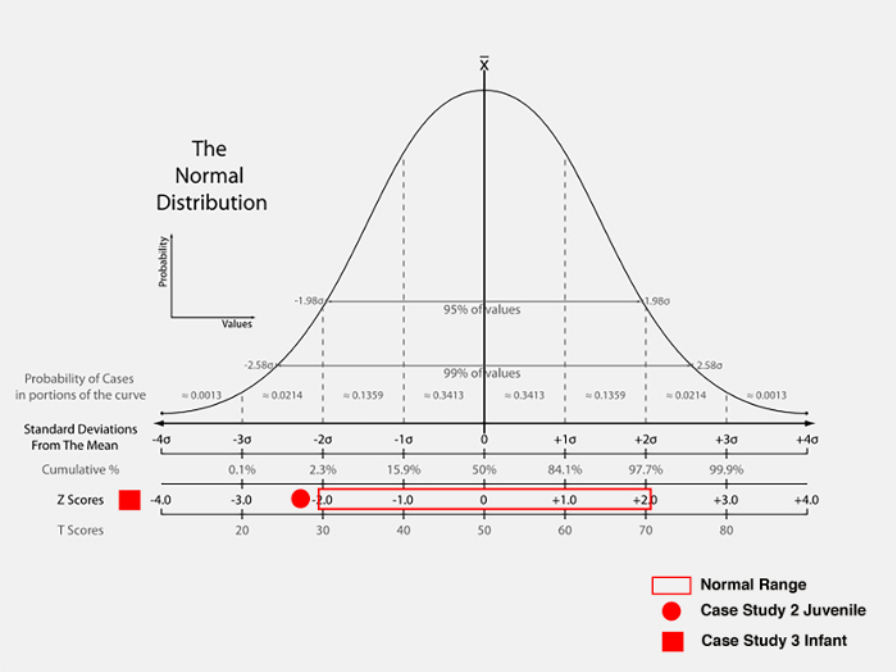

Figure 13: Assignment of case study 3 infant *z*-score relative to the normal population distribution. All values below the red center box for the normal population measures are considered to indicate low BMD for chronological age. Please click here to view a larger version of this figure.

(B)

DXA Results Summary:

Region	Area (cm^2)	BMC (g)	BMD (g/cm^2)	T-score	PR (%)	Z-score	AM (%)
L1	1.59	0.45	0.284		28		
L2	1.96	0.45	0.230		21		
L3	2.46	0.47	0.190		17		
L4	2.95	0.33	0.113		10		
Total	**8.97**	**1.70**	**0.190**		**17**		

Figure 14: BMD results for *Case Study 3.* The results presented here are from a deceased male infant, 14 months of age. Report has been anonymized for publication. (A) presents scan of AP lumbar vertebrae for *Case Study* 3 separated bone map of vertebral body epiphyses and surrounding vertebral processes; (B) scan results present the individual vertebrae and total BMD scores. The manufacturer's database used by this software did not have any age- and sex-matched information for infants younger than three years of age. References from Braillon and colleagues[91] were used to calculate the *z*-score.

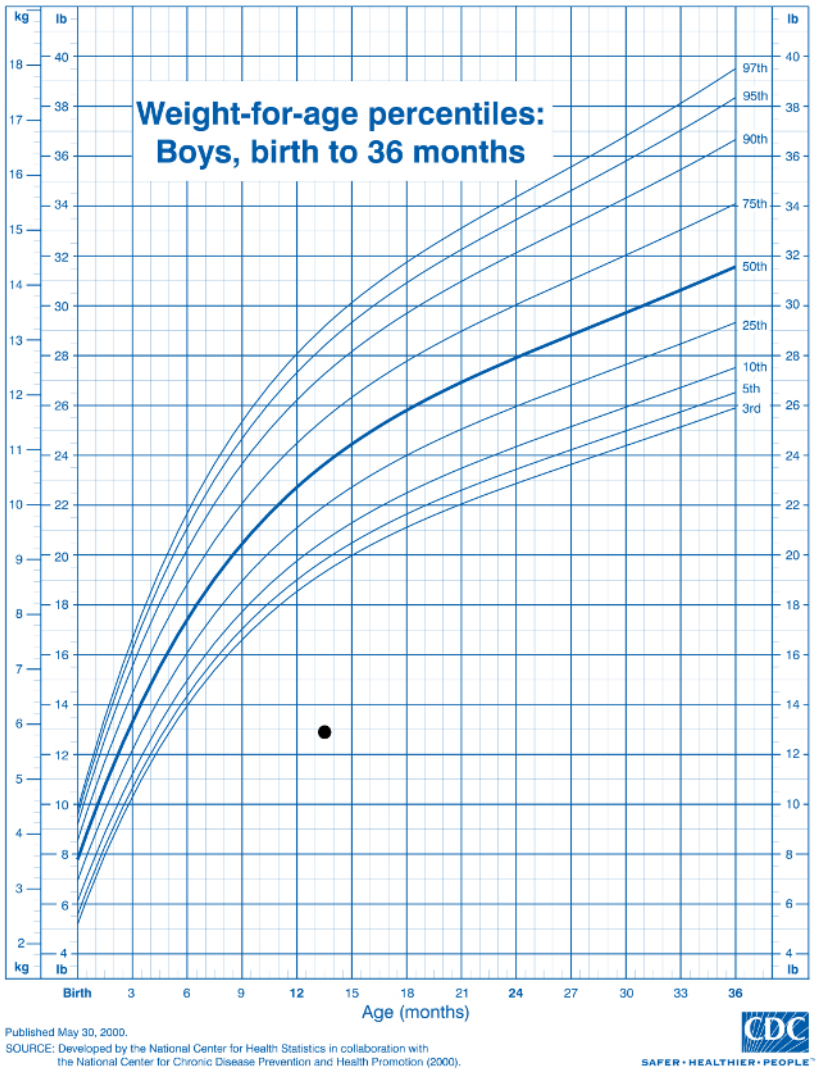

Figure 1. Individual growth chart 3rd, 5th, 10th, 25th, 50th, 75th, 90th, 95th, 97th percentiles, birth to 36 months: Boys weight-for-age

Figure 15: Growth chart illustrating the severe wasting of the 14-month-old infant.[41] The black dot represents the 6.1 kg (13.4 lbs) weight of the infant. The infant falls well below the 3rd percentile for weight-for-age. Please click here to view a larger version of this figure.

Discussion

The results presented in this paper are illustrative of the applicability of BMD metrics in forensic contexts. As **Figure 6** and **Figure 8** show, the scanning position of living individuals for clinical BMD scans is reproducible with skeletal remains, but care must be taken to ensure proper positioning. This is especially critical for the hip examination where identifying the midline of the femoral neck require the proper angle of the femur and overestimation of BMD can occur if the iliac tuberosity is not properly positioned medially to the acetabulo-femoral joint. For the adult male discussed in *Case Study 1*, BMD metrics can provide the caseworker with additional information about possible pathological conditions. Without a measure of BMD, the longitudinal fractures could have been consistent with bone insufficiency. This also illustrates that BMD assessment can be advantageous over X-rays for discerning possible fracture etiologies.

Case Study 2 and *3* provide instances where BMD metrics were integral to establishing severe malnutrition that supported more commonly used methods. Juvenile cases of fatal starvation are difficult to identify and prosecute especially when remains are recovered in advanced stages of decomposition[31,37,38]. The addition of DXA scanning protocols when fatal starvation is suspected can provide further support for findings. In both juvenile case studies, DXA scans were applied in conjunction with standard methods to compare these individuals with living children. Indeed, in both cases the DXA results were consistent with the standard method findings illustrating its usefulness in forensic cases of fatal starvation or neglect. Overall, the three cases discussed here were bolstered by DXA analysis to either include or exclude certain inferences about each case. However, there are limitations to when this method should be applied in forensic contexts. For example, research has shown that the relationship between bone volume and bone area in juveniles varies between growth stages[12,92]. Ensuring that the proper methodology and normative data is being used (*i.e.*, age-matched normative data) is imperative. When assessing infants, comparison to other methodologies, such as measurements of limb segments, should be included in the practitioner's assessment[25,33].

One of the main limitations of this method is the consideration of taphonomy (*i.e.*, diagenetic changes to skeletal composition after death). This relates to the estimation of survivorship of skeletal elements. In general, skeletal elements with higher BMD values during life will preserve more readily[7,27], but this does not exclude the likelihood that the bone mineral has been altered over time. Thus, while BMD can be employed bioarchaeologically to assess general levels of survivorship it should not be interpreted as living BMD-at-death. This is because if remains have been diagenetically altered, the BMC will not be an accurate reflection of BMD during life if mineral exchange or catabolism has occurred[55]. For example, Ross and Juarez[85] present a case where infanticide was suspected that may have been due to fatal starvation. However, traditional methods were chosen because the friability of the remains suggested extensive taphonomic alteration as the remains had been buried for approximately four years beneath a shed prior to discovery[85]. Thus, as mentioned previously, the taphonomic alteration would have not been an accurate reflection of the infant's BMD at death. In closing, this method can provide support for other indicators of malnutrition or metabolic bone pathologies, however, condition of remains should be assessed before interpreting DXA results in skeletal remains.

Disclosures

The authors declare no competing financial interests.

Acknowledgements

The authors would like to acknowledge the editorial reviewers as well as the two anonymous reviewers. Their suggestions and critiques were valid, much appreciated and vastly improved the original manuscript.

References

1. Ragsdale, B.D., & Lehmer, L.M. A Knowledge of Bone at the Cellular (Histological) Level is Essential to Paleopathology. In: *A Companion to Paleopathology.* Grauer, A.L., ed., Wiley-Blackwell, 225-249 (2011).
2. Burr, D., & Akkus, O. Bone Morphology and Organization. In: *Basic and Applied Bone Biology.* Burr, D., & Allen, M., eds., Elsevier/Academic Press, Amsterdam, 3-25 (2013).
3. Hall, B.K. *Bones and Cartilage.* Academic Press, US (2015).
4. Yeni, Y.N., Brown, C.U., & Norman, T.L. Influence of Bone Composition and Apparent Density on Fracture Toughness of the Human Femur and Tibia. *Bone.* **22** (1), 79-84 (1998).
5. Glimcher, M.J. The Nature of the Mineral Phase in Bone: Biological and Clinical Implications. In: *Metabolic Bone Disease and Clinically Related Disorders (Third Edition).* Avioli, L.V., & Krane, S.M., eds., Academic Press, San Diego, 23-52 (1998).
6. Bevier, W.C., Wiswell, R.A., Pyka, G., Kozak, K.C., Newhall, K.M., & Marcus, R. Relationship of body composition, muscle strength, and aerobic capacity to bone mineral density in older men and women. *J. Bone Miner. Res.* **4** (3), 421-432 (1989).
7. Lyman, R.L. Bone Density and Bone Attrition. In: *Manual of Forensic Taphonomy.* Pokines, J.T., & Symes, S.A., eds., CRC Press, Boca Raton, FL, 51-72 (2014).
8. Vogel, K.A., *et al.* The effect of dairy intake on bone mass and body composition in early pubertal girls and boys: a randomized controlled trial. *Am. J. Clin. Nutr.* **105** (5), 1214-1229 (2017).
9. van Leeuwen, J., Koes, B.W., Paulis, W.D., & van Middelkoop, M. Differences in bone mineral density between normal-weight children and children with overweight and obesity: a systematic review and meta-analysis. *Obes. Rev.* **18** (5), 526-546 (2017).
10. Sopher, A.B., Fennoy, I., & Oberfield, S.E. An update on childhood bone health: mineral accrual, assessment and treatment. *Curr. Opin. Endocrinol. Diabetes Obes.* **22** (1), 35-40 (2015).
11. Pezzuti, I.L., Kakehasi, A.M., Filgueiras, M.T., Guimaraes, J.A., Lacerda, I.A., & Silva, I.N. Imaging methods for bone mass evaluation during childhood and adolescence: an update. *J. Pediatr. Endocrinol. Metab.* (2017).
12. Specker, B.L., & Schoenau, E. Quantitative Bone Analysis in Children: Current Methods and Recommendations. *J. Pediatr.* **146** (6), 726-731 (2005).
13. Binkovitz, L., & Henwood, M. Pediatric DXA: technique and interpretation. *Pediatr. Radiol.* **37** (1), 21-31 (2007).
14. Siris, E.S., *et al.* Identification and Fracture Outcomes of Undiagnosed Low Bone Mineral Density in Postmenopausal Women: Results From the National Osteoporosis Risk Assessment. *JAMA.* **286** (22), 2815-2822 (2001).
15. Riggs, B.L., Wahner, H.W., Dunn, W.L., Mazess, R.B., Offord, K.P., & Melton, L.J. Differential changes in bone mineral density of the appendicular and axial skeleton with aging: relationship to spinal osteoporosis. *J. Clin. Invest.* **67** (2), 328 (1981).
16. Marshall, D., Johnell, O., & Wedel, H. Meta-Analysis Of How Well Measures Of Bone Mineral Density Predict Occurrence Of Osteoporotic Fractures. *Br. Med. J.* **312** (7041), 1254-1259 (1996).
17. Majumdar, S., *et al.* Correlation of Trabecular Bone Structure with Age, Bone Mineral Density, and Osteoporotic Status: In Vivo Studies in the Distal Radius Using High Resolution Magnetic Resonance Imaging. *J. Bone Miner. Res.* **12** (1), 111-118 (1997).
18. Cundy, T., Cornish, J., Evans, M.C., Gamble, G., Stapleton, J., & Reid, I.R. Sources of interracial variation in bone mineral density. *J. Bone Miner. Res.* **10** (3), 368-373 (1995).
19. Blake, G.M., & Fogelman, I. The role of DXA bone density scans in the diagnosis and treatment of osteoporosis. *Postgrad. Med. J.* **83** (982), 509-517 (2007).
20. Blake, G.M., & Fogelman, I. An Update on Dual-Energy X-Ray Absorptiometry. *Semin. Nucl. Med.* **40** (1), 62-73 (2010).
21. Dhainaut, A., Hoff, M., Syversen, U., & Haugeberg, G. Technologies for assessment of bone reflecting bone strength and bone mineral density in elderly women: an update. *Womens Health.(Lond).* **12** (2), 209-216 (2016).
22. Patel, R., Blake, G.M., Rymer, J., & Fogelman, I. Long-Term Precision of DXA Scanning Assessed over Seven Years in Forty Postmenopausal Women. *Osteoporos. Int.* **11** (1), 68-75 (2000).
23. Amstrup, A.K., Jakobsen, N.F.B., Moser, E., Sikjaer, T., Mosekilde, L., & Rejnmark, L. Association between bone indices assessed by DXA, HR-pQCT and QCT scans in post-menopausal women. *J. Bone Miner. Metab.* **34** (6), 638-645 (2016).
24. Blake, G.M., & Fogelman, I. How Important Are BMD Accuracy Errors for the Clinical Interpretation of DXA Scans? *J. Bone Miner. Res.* **23** (4), 457-462 (2008).

25. Ross, A. Fatal Starvation/Malnutrition: Medicolegal Investigation from the Juvenile Skeleton. In: *The Juvenile Skeleton in Forensic Abuse Investigations.* Ross, A.H., & Abel, S.M., eds., Humana Press, Totowa, NJ, 151-165 (2011).
26. Ross, A., & Juarez, C. A brief history of fatal child maltreatment and neglect. *Forensic Sci. Med. Pathol.* **10** (3), 413-422 (2014).
27. Lyman, R.L. Quantitative units and terminology in zooarchaeology. *Am. Antiq.* **59** (1), 36-71 (1994).
28. U.S. Department of Health and Human Services. Child Maltreatment. *Administration for Children and Families, Administration on Children, Youth, and Families, Children's Bureau.* (2015).
29. Spitz, W.U., Clark, R., & Spitz, D.J. *Spitz and Fisher's Medicolegal Investigation of Death: Guidelines for the Application of Pathology to Crime Investigation.* Charles C Thomas, Springfield (2006).
30. Dudley, M.D., Mary, H. *Forensic Medicolegal Injury and Death Investigation.* CRC Press, Milton (2016).
31. Block, R.W., Krebs, N.F., and Committee on Child Abuse and Neglect & and Committee on Nutrition. Failure to Thrive as a Manifestation of Child Neglect. *Pediatr.* **116** (5), 1234 (2005).
32. Ross, A.H., & Abel, S.M. *The Juvenile Skeleton in Forensic Abuse Investigations.* Humana Press, Totowa, NJ (2011).
33. Damashek, A., Nelson, M.M., & Bonner, B.L. Fatal child maltreatment: characteristics of deaths from physical abuse versus neglect. *Child Abuse Negl.* **37** (10), 735 (2013).
34. Welch, G.L., & Bonner, B.L. Fatal child neglect: characteristics, causation, and strategies for prevention. *Child Abuse Negl.* **37** (10), 745-752 (2013).
35. Gosman, J. Growth and Development: Morphology, Mechanisms, and Abnormalities. In: *Bone Histology: An Anthropological Perspective.* Crowder, C., & Stout, S., eds., CRC Press, 23-44 (2011).
36. Bass, S.L., Eser, P., & Daly, R. The effect of exercise and nutrition on the mechanostat. *J. Musculoskelet. Neuronal Interact.* **5** (3), 239-254 (2005).
37. Berkowitz, C.D. Fatal child neglect. *Adv. Pediatr.* **48**, 331-361 (2001).
38. Knight, L.D., & Collins, K.A. A 25-year retrospective review of deaths due to pediatric neglect. *Am. J. Forensic Med. Pathol.* **26** (3), 221-228 (2005).
39. Ruff, C. Body size prediction from juvenile skeletal remains. *Am. J. Phys. Anthrop.* **133** (1), 698-716 (2007).
40. Cowgill, L. Juvenile body mass estimation: A methodological evaluation. *J. Hum. Evol.* (2017).
41. Kuczmarski, R.J.*, et al.* 2000 CDC Growth Charts for the United States: methods and development. *Vital and health statistics. Series 11, Data from the national health survey.* (246), 1 (2002).
42. Crabtree, N.J.*, et al.* Dual-energy X-ray absorptiometry interpretation and reporting in children and adolescents: the revised 2013 ISCD Pediatric Official Positions. *J. Clin. Densitom.* **17** (2), 225-242 (2014).
43. Crabtree, N.J., Leonard, M.B., & Zemel, B.S. Dual-energy X-ray absorptiometry. In: *Bone densitometry in growing patients. Guidelines for clinical practice.* Sawyer, A.J., Bachrach, L.K., & Lung, E.B., eds., Humana Press, Totowa, 41-57 (2007).
44. Ward, K., Mughal, Z., & Adams, J. Tools for Measuring Bone in Children and Adolescents. In: *Bone Densitometry in Growing Patients. Guidelines for clinical practice.* Sawyer, A.J., Fung, E.B., & Bachrach, L.K., eds., Humana Press, Totowa, NJ, 15-40 (2007).
45. Alp, H., Orbak, Z., Kermen, T., & Uslu, H. Bone mineral density in malnourished children without rachitic manifestations. *Pediatr. Int.* **48** (2), 128-131 (2006).
46. American College of Radiology. *ACR appropriateness criteria.* <https://acsearch.acr.org/list> (2016).
47. Leonard, C., Roza, M., Barr, R., & Webber, C. Reproducibility of DXA measurements of bone mineral density and body composition in children. *Pediatr. Radiol.* **39** (2), 148-154 (2009).
48. Carrascosa, A., Gussinye, M., Yeste, D., Audi, L., Enrubia, M., & Vargas, D. Skeletal mineralization during infancy, childhood, and adolescence in the normal population and in populations with nutritional and hormonal disorders. Dual X-ray absorptiometry (DXA) evaluation. In: *Paediatric Osteology: New Developments in Diagnostics and Therapy.* Schiinau, E., ed., 93-102 (1996).
49. Blake, G.M., Wahner, H.W., & Fogelman, I. *The Evaluation of Osteoporosis.* Martin Dunitz, London, UK (1999).
50. Christensen, A.M., Passalacqua, N.V., & Bartelink, E.J. *Forensic Anthropology: Current Methods and Practice.* Academic Press, US (2014).
51. Brickley, M., & Howell, P.G.T. Measurement of Changes in Trabecular Bone Structure with Age in an Archaeological Population. *J. Archaeol. Sci.* **26** (2), 151-157 (1999).
52. Ortner, D.J., & Putschar, W.G. *Identification of pathological conditions in human skeletal remains.* Volume 28, Smithsonian Inst. Press, Washington (1981).
53. Waldron, T. *Palaeopathology.* Cambridge Univ. Press, Cambridge (2009).
54. Kozlowski, T., & Witas, H.W. Metabolic and Endocrine Diseases. In: *A Companion to Paleopathology.* Grauer, A.L., ed., Wiley-Blackwell, 401-419 (2012).
55. Agarwal, S.C. Light and Broken Bones: Examining and Interpreting Bone Loss and Osteoporosis in Past Populations. In: *Biological Anthropology of the Human Skeleton.* Katzenberg, M.A., & Saunders, S.R., eds., John Wiley & Sons, Inc, Hoboken, NJ, USA, 387-410 (2008).
56. Mays, S., Turner-Walker, G., & Syversen, U. Osteoporosis in a population from medieval Norway. *Am. J. Phys. Anthropol.* **131** (3), 343-351 (2006).
57. McEwan, J.M., Mays, S., & Blake, G.M. The relationship of bone mineral density and other growth parameters to stress indicators in a medieval juvenile population. *Int. J. Osteoarchaeol.* **15** (3), 155-163 (2005).
58. McEwan, J.M., Mays, S., & Blake, G.M. Measurements of Bone Mineral Density of the Radius in a Medieval Population. *Calcif. Tissue Int.* **74** (2), 157-161 (2004).
59. Lees, B., Stevenson, J.C., Molleson, T., & Arnett, T.R. Differences in proximal femur bone density over two centuries. *Lancet.* **341** (8846), 673-676 (1993).
60. Agarwal, S.C., & Grynpas, M.D. Measuring and interpreting age-related loss of vertebral bone mineral density in a medieval population. *Am. J. Phys. Anthropol.* **139** (2), 244-252 (2009).
61. Farquharson, M.J., & Brickley, M. Determination of mineral make up in archaeological bone using energy dispersive low angle X-ray scattering. *Int. J. Osteoarchaeol.* **7**, 95-99 (1997).
62. Wakely, J., Manchester, K., & Roberts, C. Scanning electron microscope study of normal vertebrae and ribs from early medieval human skeletons. *J. Archaeol. Sci.* **16** (6), 627-642 (1989).
63. Brickley, M., & Ives, R. *The Bioarchaeology of Metabolic Bone Disease.* Academic Press, Oxford (2010).
64. Kneissel, M., Boyde, A., Hahn, M., Teschler-Nicola, M., Kalchhauser, G., & Plenk, H. Age- and sex-dependent cancellous bone changes in a 4000y BP population. *Bone.* **15** (5), 539-545 (1994).

65. Fan, B., *et al.* National Health and Nutrition Examination Survey whole-body dual-energy X-ray absorptiometry reference data for GE Lunar systems. *J. Clin. Densitom.* **17** (3), 344-377 (2014).
66. Kanis, J.A., McCloskey, E.V., Johansson, H., Odén, A., Melton, L.J., & Khaltaev, N. A reference standard for the description of osteoporosis. *Bone.* **42** (3), 467-475 (2008).
67. Looker, A.C., Borrud, L.G., Hughes, J.P., Fan, B., Shepherd, J.A., & Melton, J.L. Lumbar spine and proximal femur bone mineral density, bone mineral content, and bone area: United States, 2005-2008. *Vital and health statistics 11.* **251**, 1-132 (2012).
68. Beck, T.J., Looker, A.C., Ruff, C.B., Sievanen, H., & Wahner, H.W. Structural Trends in the Aging Femoral Neck and Proximal Shaft: Analysis of the Third National Health and Nutrition Examination Survey Dual-Energy X-Ray Absorptiometry Data. *J. Bone Miner. Res.* **15** (12), 2297-2304 (2000).
69. Humphries, A.L., Maxwell, A.B., Ross, A.H., & Privette, J. Skeletal Trauma Analysis in the Elderly: A Case Study on the Importance of a Contextual Approach. *67th Annual Proceedings of the American Academy of Forensic Sciences.*, 862 (2015).
70. Willey, P., Galloway, A., & Snyder, L. Bone mineral density and survival of elements and element portions in the bones of the Crow Creek massacre victims. *Am. J. Phys. Anthropol.* **104** (4), 513-528 (1997).
71. Galloway, A., Willey, P., & Snyder, L. Human bone mineral densities and survival of bone elements: A contemporary sample. In: *Forensic Taphonomy: The Postmortem Fate of Human Remains.* Haglund, W.D., & Sorg, M.H., eds., CRC Press, Boca Raton, FL, 295-317 (1997).
72. Symmons, R. Digital photodensitometry: a reliable and accessible method for measuring bone density. *J. Archaeol. Sci.* **31** (6), 711-719 (2004).
73. Boaz, N.T., & Behrensmeyer, A.K. Hominid taphonomy: transport of human skeletal parts in an artificial fluviatile environment. *Am. J. Phys. Anthropol.* **45** (1), 53-60 (1976).
74. Behrensmeyer, A.K. The Taphonomy and Paleoecology of Plio-Pleistocene Vertebrate Assemblages East of Lake Rudolf, Kenya. *Bull. Mus. Comp. Zool.* **146**, 473-578 (1975).
75. Lyman, R.L. Bone density and differential survivorship of fossil classes. *J. Anthropol. Archaeol.* **3** (4), 259-299 (1984).
76. Lam, Y.M., & Pearson, O.M. Bone density studies and the interpretation of the faunal record. *Evol. Anthropol.* **14** (3), 99-108 (2005).
77. Lam, Y.M., Chen, X., & Pearson, O.M. Intertaxonomic variability in patterns of bone density and the differential representation of bovid, cervid, and equid elements in the archaeological record. *Am. Antiq.* **64** (2), 343 (1999).
78. Lam, Y.M., Chen, X., Marean, C.W., & Frey, C.J. Bone Density and Long Bone Representation in Archaeological Faunas: Comparing Results from CT and Photon Densitometry. *J. Archaeol. Sci.* **25** (6), 559-570 (1998).
79. Symmons, R. New density data for unfused and fused sheep bones, and a preliminary discussion on the modelling of taphonomic bias in archaeofaunal age profiles. *J. Archaeol. Sci.* **32** (11), 1691-1698 (2005).
80. Pickering, T.R., & Carlson, K.J. Baboon Bone Mineral Densities: Implications for the Taphonomy of Primate Skeletons in South African Cave Sites. *J. Archaeol. Sci.* **29** (8), 883-896 (2002).
81. Ioannidou, E. Taphonomy of Animal Bones: Species, Sex, Age and Breed Variability of Sheep, Cattle and Pig Bone Density. *J. Archaeol. Sci.* **30** (3), 355-365 (2003).
82. Hale, A.R., & Ross, A.H. The Impact of Freezing on Bone Mineral Density: Implications for Forensic Research. *J. Forensic Sci.* **62** (2), 399-404 (2017).
83. WHO Study Group. *Assessment of fracture risk and its application to screening for postmenopausal osteoporosis.* Volume 843, World Health Organization, Geneva (1995).
84. Symes, S.A., L'Abbe, E.N., Stull, K.E., Lacroix, M., & Pokines, J.T. Taphonomy and the Timing of Bone Fractures in Trauma Analysis. In: *Manual of Forensic Taphonomy.* Pokines, J.T., & Symes, S.A., eds., CRC Press, Taylor and Francis Group, Boca Raton, FL, 341-366 (2014).
85. Ross, A.H., & Juarez, C.A. Skeletal and radiological manifestations of child abuse: Implications for study in past populations. *Clin. Anat.* **29** (7), 844-853 (2016).
86. Feldesman, M.R. Femur/stature ratio and estimates of stature in children. *Am. J. Phys. Anthropol.* **87** (4), 447-459 (1992).
87. Anderson, M., Green, W., & Messner, M. Growth and predictions of growth in the lower extremities. *J. Bone Joint Surg. Am.* **45** (A), 1-14 (1963).
88. Kelly, T.L., Specker, B.L., Binkely, T., & et al. Pediatric BMD reference database for US white children. *Bone (Suppl).* **36** (O-15), S30 (2005).
89. Gomez, F., Galvan, R., Cravioto, J., & Frenk, S. Malnutrition in infancy and childhood with special reference to Kwashiokor. *Adv. Pediatr.* **7**, 131-169 (1955).
90. Waterlow, J.C. Classification and definition of protein-caloric malnutrition. *Br. Med. J.* **2**, 566-569 (1972).
91. Braillon, P.M., Salle, B.L., Brunet, J., Glorieux, F.H., Delmas, P.D., & Meunier, P.J. Dual energy x-ray absorptiometry measurement of bone mineral content in newborns: validation of the technique. *Pediatr. Res.* **32** (1), 77-80 (1992).
92. Gallo, S., Vanstone, C.A., & Weiler, H.A. Normative data for bone mass in healthy term infants from birth to 1 year of age. *J. Osteoporos.* **2012**, 672403 (2012).

